Helical Crystal Assemblies in Nonracemic Chiral Liquid Crystalline Polymers: Where Chemistry and Physics Meet†

Jing Wang,‡ Christopher Y. Li,§ Shi Jin,‡ Xin Weng,‡ Ryan M. Van Horn,‡ Matthew J. Graham,‡ Wen-Bin Zhang,‡ Kwang-Un Jeong,|| Frank W. Harris,‡ Bernard Lotz,⊥ and Stephen Z. D. Cheng*,‡

College of Polymer Science and Polymer Engineering, Department of Polymer Science, The University of Akron, Akron, Ohio 44325-3909, Department of Materials Sciences and Engineering, Drexel University, Philadelphia, Pennsylvania 19014, Department of Polymer-Nano Science and Technology, Chonbuk National University, Jeonju, 561-756, Korea, and Institute Charles Sadron, CNRS, 6 Rue Boussingault, Strasbourg

Chirality transfer (or amplification) in soft materials is an important topic for understanding how chiral assemblies develop from the atomic level to macroscopic objects. This is an interdisciplinary area which is critically associated with the evolution from asymmetric chemistry to asymmetric physics, and, more specifically, in biomaterials, liquid crystals, and polymers. In this review, we discuss our recent studies on the conditions for chirality transfer across different length scales. We observed that the formation of helical structures in different length scales is a typical process in chirality transfer. This is illustrated by a series of nonracemic chiral main-chain liquid crystalline (LC) polyesters, PETs(R*-*n*). The polymers contained a different number of methylene units in the chain backbone (from 7 to 11). All of the PETs(R*-*n*) macroscopically exhibited an LC chiral smectic C (S_C^*) phase, a chiral smectic A (S_A^*) phase, and a twist grain boundary smectic A (TGBA*) phase with increasing temperature. The atomic chiral centers caused the helical conformation, and then, helical lamellar crystals were found in these polymers. The crystal structures were determined by X-ray diffraction and electron diffraction techniques. Dark field transmission electron microscopic images revealed that the molecular orientation in these helical crystals is double twisted. Our systematic studies showed that chirality transfer from one length scale to another is neither automatic, nor necessary, and it critically depends upon the packing scheme of the chiral building blocks on each length scale. It was particularly surprising that in this series of polyesters, the odd−even effect exists across many length scales. This includes not only thermodynamic properties such as the S_C^*, the S_A^*, and the TGBA* LC phase transition temperatures, but also the helical crystal handedness.

Introduction

Chirality on Different Length Scales. Chirality within molecules has generated new phase structures, transition behaviors, and specific optical and electronic properties in polymers,[1−13] amphiphilic molecules,[14−18] and liquid crystals.[19−31] Due to their long chain nature, chirality in polymers can be defined on different length scales, forming the hierarchy of chirality shown in Figure 1. Chiral centers in a polymer backbone, which is a primary chiral structure (configurational chirality) on a fractions-of-nanometers scale, usually results in helical macromolecular conformations (a secondary chiral structure, conformational chirality) on a nanometer scale. When the polymer chains with helical conformations pack together following symmetry operations to form ordered structures, the chirality may break the local mirror symmetry and lead to a helical building block (a tertiary chiral structure, phase chirality) on a micrometer scale depending on the type of structural ordering formed. The helical building blocks may aggregate to form chiral entities on a larger macroscopic length scale, and this is identified as a quaternary chiral structure, defined as object chirality in Figure 1.[32]

The primary chiral structures result from the asymmetric chemical connections of atoms, while chirality on longer length scales is due to physical interactions. The development of asymmetric synthesis in the past two decades allows us to design and control the chiral structure at the primary level. This leads to the possibility of investigating chirality transfer across length scales into higher hierarchies. This hierarchical approach may lead to further understanding of chirality transfer in biomolecules and, even further, in living systems.

In the past, research interest in high-level chiral structures (phase chirality and object chirality) has focused on three areas: polymers including copolymers and biopolymers, amphiphilic molecules and liquid crystals. In polymers, poly(hydroxybu-

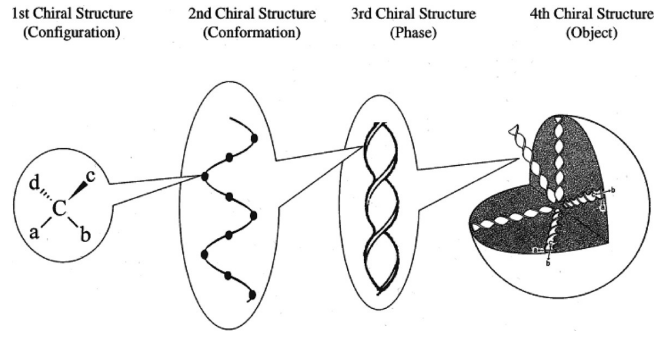

Figure 1. Four levels of chirality in polymers.[32] The primary (configuration) chirality is on a fractions-of-nanometers scale; the secondary (conformation) chirality is on a nanometer scale; the tertiary chirality (phase) is on a micrometer scale, and the quaternary chirality is on a larger macroscopic length scale.

† On the occasion of the 70th birthday of Prof. Don Paul for his exceptional contribution to polymer science and engineering.

* To whom correspondence should be addressed. E-mail: scheng@uakron.edu.

‡ The University of Akron.

§ Drexel University.

|| Chonbuk National University.

⊥ Institute Charles Sadron.

10.1021/ie100248r © 2010 American Chemical Society
Published on Web 03/26/2010

tyrate) (PHB), obtained from natural bacterial sources with the R(−) enantiomer, and the R(−) enantiomer of poly(propylene oxide) (PPO) are both crystallizable nonracemic chiral polymers that usually form banded spherulites due to cooperative lamellar twisting. It should be noted that the banded spherulites are formed due to this cooperative lamellar twisting, not due to chirality, such as in the case of polyethylene (PE) and other nonchiral polymers (see below). If the twisted lamellar crystals are considered a tertiary chiral structure, the banded spherulites correspond to the highest level of naturally occurring chiral structures, i.e., the quaternary chiral structure (Figure 1) in polymer systems.[2,3] It has been frequently speculated that the helical sense of these banded spherulites must be associated with the chiral configuration of the polymer chains. However, PHB with the R(−) enantiomer exhibits right-handed banded spherulites.[2] Contrary to the PHB case, the R(−) enantiomer of PPO generates left-handed banded spherulites, while PPO with the S(+) enantiomer forms left-handed banded spherulites. In a 50:50 mixture of R(−) and S(+) enantiomers, the banded texture disappears in the spherulites.[4] Therefore, the chiral configuration of the polymer backbones should play an important role in the handedness of banded spherulites. Furthermore, a recent study shows that unlike banded spherulites, lamellar single crystals of optically active R(−) or S(+) poly(epichlorohydrin) grown from dilute solution are flat.[3−6] In other words, the conformational chirality is not transferred to the phase chirality, and thus, the chiral memory is somehow lost between these two structural hierarchies.

All biopolymers possess primary nonracemic chiral structures, since the information density on a chemical group is increased by introducing a chiral structure, which makes economic use of space and materials. A well-known example is that the β-sheet conformation, a common class of structures consisting of hydrogen bonding within the sheets, as first proposed by Pauling and his colleagues, and confirmed using wide-angle X-ray diffraction (WAXD).[7,8] The neighboring chiral chain packing of these β-sheets in the globular proteins are twisted and deviate from a 2_1 symmetry along the long axis of the sheet based on the local conformational calculations.[9] Therefore, the twisted sheets possess a lower free energy than those possessing a 2_1 symmetry. This was observed in the case of globular proteins wherein several β-pleated sheets are embedded into a relatively less-ordered environment.[10] In the early 1980s, it was also found that *Bombyx mori* silk fibroin can grow a helical lamellar crystal of the β-modification from solution crystallization.[11] In another example, dinoflagellate chromosomes (in *Prorocentrum micans*) in an in vivo arrangement also displayed the same type of helical structure[12] although it only deals with protein molecular packing in a less ordered form rather than a crystal form as in the case of *Bombyx mori* silk fibroin.

On the basis of these examples, it is evident that one cannot correlate the primary chiral structure with the quaternary chiral structure without knowing the secondary and tertiary chiral structures. In other words, *transfer from one chirality length-scale or hierarchical structure to the next is neither automatic nor necessary.* Establishing quantitative links for chirality transfer across these hierarchical length-scales requires information on the conformational and phase chiralities. Furthermore, configurational chirality is not necessarily the only cause of lamellar twisting. An example of this phenomena is nonchiral PE, as indicated previously. There are a number of reasons for twisting in lamellae. Most of these reasons are based on the unbalanced surface stresses between the two lamellar basal surfaces introduced by the structural asymmetry in these lamellar crystals. Such unbalanced surface stresses cause a significant longitudinal bending moment in the crystals and causes the lamellar twisting.[13,33]

Molecular chirality was also found to be critical in inducing the curvature of amphiphilic membranes.[14−18] This is of special interest not only for material design, but also in the field of molecular biology, since the highly folded lipid bilayers are a major component of the plasma membrane system in eukaryotic cells. Many chiral amphiphilic molecules can aggregate into four types of ribbonlike morphologies:[14,15] flat ribbons, helices A (wound ribbons with a cylindrical curvature), helices B (twisted ribbons with a saddlelike curvature), and tubes. Most of these chiral amphiphiles are small molecules, and thus, the importance of the secondary chiral structure (conformational chirality) may be less obvious. Yet, transfer of chirality between different length scales is also not necessary. Most chiral amphiphiles can form flat ribbons, which are achiral,[15] while an achiral anhydride forms equal numbers of left- and right-handed helices during crystallization.[16] Similar self-assembling behavior was also found in amphiphilic diblock copolymers (see refs 17 and 18 for example). To understand the formation mechanism of these chiral morphologies in amphiphilic membranes, detailed information concerning the molecular packing scheme must be obtained.

Poly(L- and D-lactic acid)s (PLLA or PDLA), on the other hand, are polymers with nonracemic chiral centers. Single crystals of these homopolymers are flat and show no sign of chiralty transfer to the tertiary chiral structure, except in the thin film case. However, their diblock copolymers with polystyrene (PS) at a volume fraction where the PS block is in the majority and the PLLA or PDLA forms the cylindrical

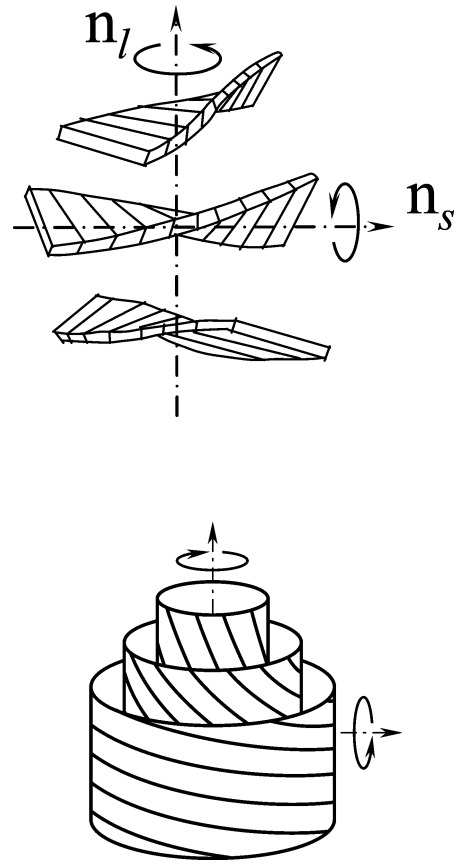

Figure 2. Two types of double-twisted geometry.

nanophase morphology exhibit chiral helical structures in the bulk PS matrix prior to the formation of the crystalline state.[34−37]

Chiral liquid crystalline (LC) materials exhibit a number of different phases based on their order and symmetry.[19] Helical structures are well-known in low-ordered liquid crystalline phases, such as in cholesteric (Ch) phases, blue phases (BP), twisted grain boundary phases (TGB), and the smectic C* (S_C^*) phase,[19] as well as the surface-induced ferroelectricity in the S_C^* phase.[20] In the helical morphologies of Ch[21,22] and TGB phases,[23−25] the long direction of the geometrically anisotropic molecules is usually perpendicular to the helical axis, while in S_C^* phases, the long direction generally possesses an acute angle with respect to the helical axis.[26] Helical arrangements have also been identified in BPs in which the direction of the helical axis changes with respect to the long molecular direction.[27] In the condensed states of synthetic LC materials, tertiary helical structures have only been found in low-ordered LC phases. As the structural order increases to form highly ordered LC phases (such as smectic crystal G*, H*, J*, and K* phases), the helical arrangements are expected to be suppressed.[19] This is because the interactions generating the helical packing are typically lower than the interactions forming high-ordered phases (such as during crystallization). The latter case requires a parallel close packing scheme.[19] Therefore, in these highly ordered smectic crystal phases in chiral liquid crystals, the phase morphologies are not different from their nonchiral counterparts. No helical arrangements can be observed. Hence, the chirality transfer is "lost" at the tertiary level.

On the other hand, there is a recent study for a series of biphenyl carboxylic acid compounds which can construct dimers via hydrogen bonds to form liquid crystals. These series of liquid crystalline dimers do not contain a chiral center in the atomic scale, yet they can form a helical morphology in their smectic C phase because of volume confinement of the liquid crystalline texture[38,39] and subsequent construction of chiral propeller architectures in droplets.[40] All of these are due to the fact that conformations of these dimers possess chirality.[39]

There are two categories of molecular arrangement in the tertiary helical structures. The first type is the double-twisted geometry as shown in Figure 2a wherein only a single center parent sheet of constant thickness is shown. The parent sheet can be built from the continuous helical rotation of elongated units which simultaneously follow a translation along the long axis of the sheet. The cross-section of this twisted sheet is not exactly rectangular in shape. Many of these helical sheets stack on both sides of the parent sheet. Between the neighboring sheets, another continuous helical rotation exists along an axis that is perpendicular to the long helical axis. One thus obtains a double-twisted geometry.[28] There is another double-twisted geometry with a cylindrical packing, which corresponds to compact stacking of elongated molecules with a helical conformation along the cylindrical direction (Figure 2b).[29] The chain molecules, on a local scale, are not parallel, but equidistant. It

Scheme 1

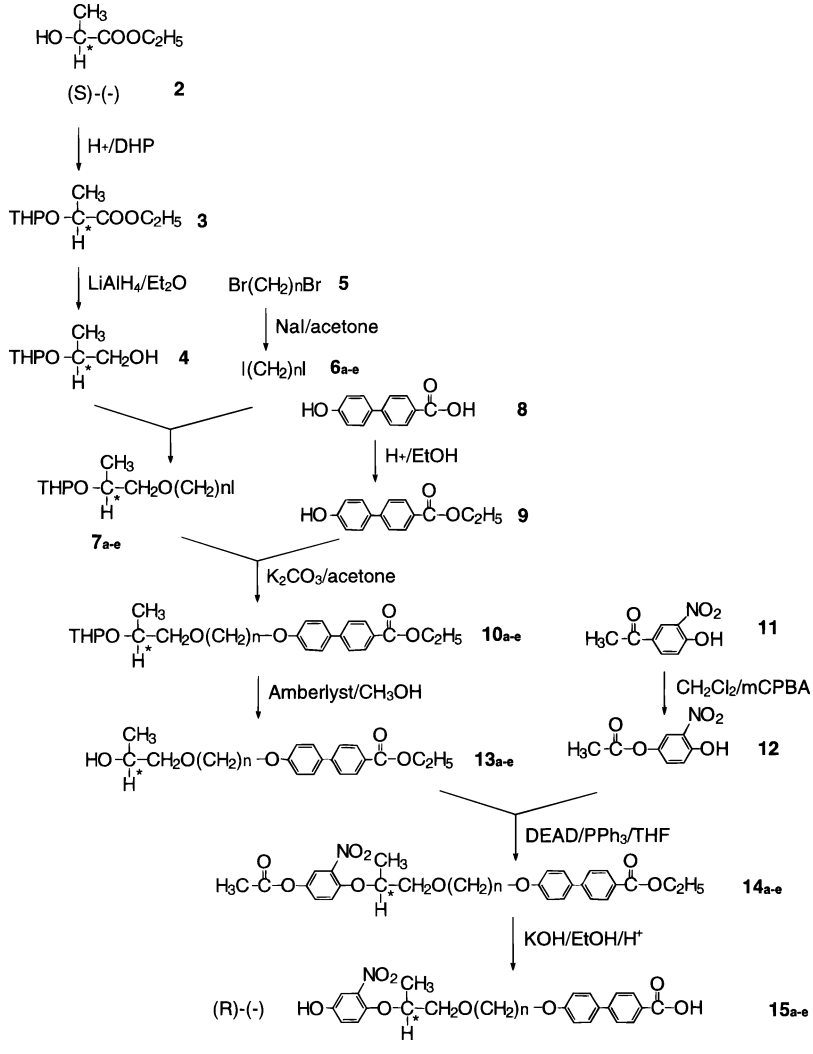

Scheme 2

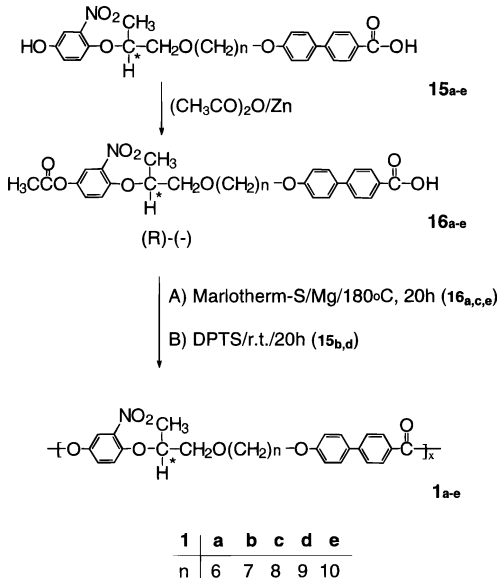

is evident that geometric frustration occurs when competition exists between the tendencies toward molecular parallel alignment and chiral configuration. Experimentally, the double-twisted geometry shown in Figure 2b has been observed in biological polymers such as DNA, polysaccharides (xanthan) and polypeptides (poly-γ-butyl-L-glutamate) in both in vitro and in vivo arrangements.[30] It should be noted that most of these biological polymers are in a LC rather than a crystalline phase.[31]

From all the experimental observations in these three areas, it has been recognized that the chirality transfer is an important topic, yet we are some distance away from complete understanding. In particular, it is necessary to investigate how the molecules (or chains) and building blocks on different length scales pack with each other to construct the chiral helical arrangements, which requires detailed structural analysis and molecular packing schemes in each of the chiral hierarchies.

In order to systematically investigate chirality transfers, we designed and synthesized a series of chiral nonracemic model compounds with atomic chirality on the primary level and helical conformation on the secondary level. It was to our surprise that helical single lamellar crystals on the third level of chirality have been observed. To our knowledge, this was the first time in synthetic polymers that a tertiary chiral structure with a helical morphology was preserved in the crystalline state. This set of polymers provided an opportunity to understand how chirality is transferred from one hierarchical length scale to another. Studying their ternary and quaternary chiral structures enabled us to analyze the detailed molecular packing in the chiral phase and understand the chirality transfer process.[28]

Synthesis of Nonracemic Chiral Polyesters. For the past several years, we have studied a series of nonracemic chiral main-chain liquid crystalline (LC) polyesters synthesized from (R)-(−)-4′-{ω-[2-(*p*-hydroxy-*o*-nitrophenyloxy)-1-propyloxy]-1-alkyloxy}-4-biphenyl carboxylic acids. The general structure of the chemical repeat unit is the following:

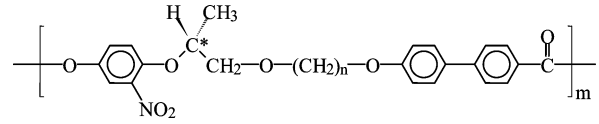

The polymers are abbreviated as PET(R*-*n*), where *n* is the number of methylene units.[28,41−43] Detailed monomer and polymer synthetic routes can be found in ref 35. Scheme 1 summarizes the synthetic route of the monomers. The polymers were prepared from the carboxylic acid derivatives of the monomers, as reported by Economy et al.[44] However, harsh reaction conditions, such as at high temperatures (about 300−350 °C). Two methods were used to produce the polymer under relatively mild conditions, as shown in Scheme 2. Samples of PET(R*-8) and PET(R*-10) were prepared via method A, resulting in relatively low-molecular-weight products (number average molecular weight M_n < 10 kg/mol). Samples of PET(R*-7), PET(R*-9), and PET(R*-11) were prepared via method B, resulting in polymers with M_n around 16−30 kg/mol. The polydispersity of all samples was approximately 2 after fractionation, as measured by gel permeation chromatography based on polystyrene standards.

This series of polymers possess right-handed chiral centers (R*) along the main-chain backbone. The left-handed chiral center (L*) has also been synthesized in order to compare the effect of configurational chirality on other length scales of chirality. The number of methylene units ranged from seven to eleven. Due to the head-to-tail connection of the monomers in this polymer from the A−B monomer polymerization,[43] the optical activity of the monomer is retained, and the polymers are nonracemic.

Identification of Liquid Crystalline Phases. Figure 3a and b show one set of cooling and one set of subsequent heating differential scanning calorimetry (DSC) thermal diagrams for

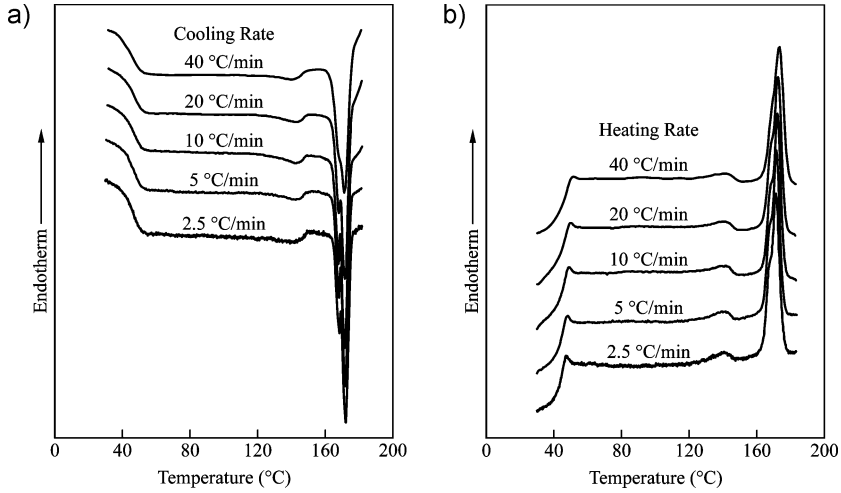

Figure 3. Sets of DSC cooling (a) and heating (b) thermodiagrams at different rates ranging from 0.5 to 40 °C/min for PET(R*-11).[46]

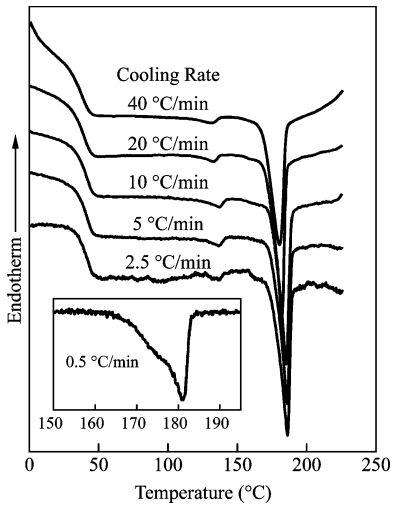

Figure 4. Set of DSC cooling thermodiagrams at different rates between ranging from 0.5 and 40 °C/min for PET(R*-9).[45]

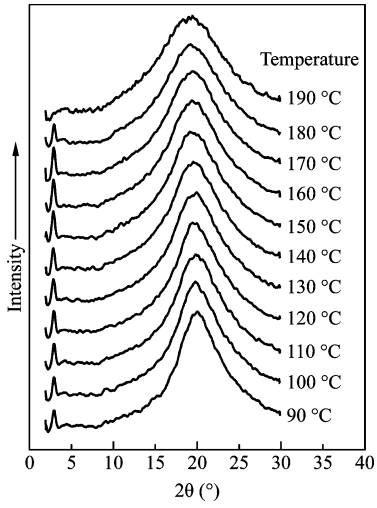

Figure 5. Set of 1D WAXD patterns at different temperatures during cooling at 20 °C/min.[45]

PET(R*-11) at different rates between 2.5 and 40 °C/min. In this cooling and heating rate range studied, there are three first-order transitions with onset transition temperatures of 163, 158, and 130 °C measured during cooling, respectively. The enthalpy changes of these three first-order transitions are 3.64 kJ/mol for the highest temperature transition and 1.29 kJ/mol for the middle temperature transition and a small transition enthalpy change (0.52 kJ/mol) at the lowest temperature of 130 °C. All three transitions are almost cooling and heating rate independent in the range of rates investigated, indicating that these transitions are associated with LC phase transformations. Other members of this series of polymers exhibit similar thermodynamic transition behaviors. Figure 4 shows a set of cooling DSC thermal diagrams for PET(R*-9).[45] The slight difference in this figure compared with Figure 3 is that the two higher temperature transitions are now merged. They can be separated only at even slower cooling rates such as at 0.5 °C/min.

Figure 5 shows a set of one-dimensional (1D) wide-angle X-ray diffraction (WAXD) patterns during fast cooling from the isotropic melt to room temperature at a rate of 20 °C/min for PET(R*-9) (see the corresponding DSC diagram in Figure 4).[45] It is evident that the LC phases cannot be bypassed at this cooling rate since the LC phase transitions are close to thermodynamic equilibrium. The 1D WAXD pattern at 190 °C

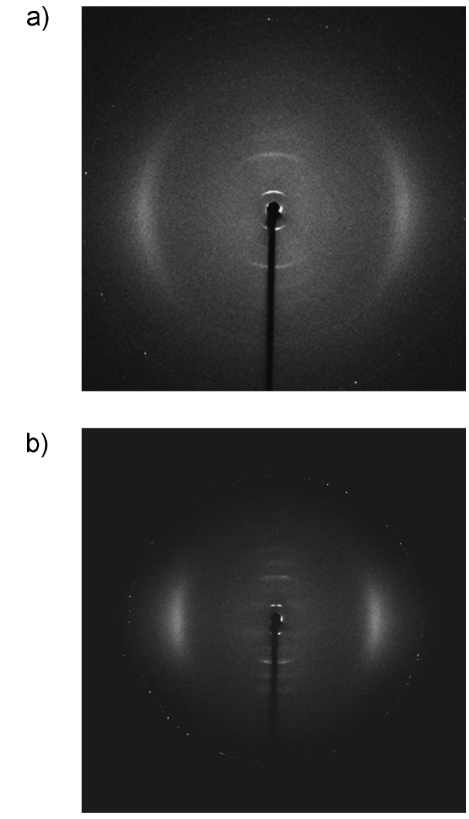

Figure 6. 2D WAXD patterns for S_A^* (a) and S_C^* (b) phases of the PET(R*-9) sample.[45]

exhibits two characteristic features as evidence of the transition. The first feature is the appearance of a low-angle reflection at $2\theta = 3.0°$ (d-spacing of 2.96 nm). The second is a sudden shift of the wide-angle halo at around $2\theta = 20°$. Both features indicate a transition from the isotropic melt to a low ordered smectic LC phase.[45] When the temperature is continuously decreased to 130 °C, the low-angle reflection exhibits a sudden shift to a slightly higher angle of $2\theta = 3.05°$ (d-spacing of 2.90 nm). Furthermore, the wide-angle scattering halo becomes increasingly sharper on cooling to below 130 °C. This transition corresponds to the small exothermic process in the DSC cooling thermal diagram (Figure 4).

In order to precisely identify the structure of these LC phases, we conducted 2D WAXD experiments at different temperatures. Figure 6a shows a 2D WAXD pattern at 160 °C, and the LC phase was determined to be a smectic A* (S_A^*) phase (note that the symmetry of this S_A^* phase is identical to normal S_A phase), since the low-angle layer reflection is on the equator and the scattering halo is on the meridian. However, Figure 6b shows a 2D WAXD pattern after annealing at 120 °C, in which the scattering halo is on the meridian while the layer reflection is slightly shifted to the quadrant. This feature is characteristic of a smectic C* (S_C^*) pattern. The angle between the layer reflection and the meridian (the fiber direction) is 79°, indicating that the layer normal is tilted 11° away from the meridian. Therefore, the transition at 130 °C is a $S_A^* \leftrightarrow S_C^*$ transition.[45]

The S_A^* and S_C^* assignments are also supported by texture observations in polarized light microscopy (PLM) in the relevant temperature regions. The film sample was sheared and relaxed at 180 °C and then slowly cooled (1 °C/min) and annealed at 160 and 120 °C, respectively. Figure 7a shows a focal conic texture formed during annealing at 160 °C; this texture is typical for a S_A^* phase. This texture becomes broken when the sample is cooled down past the $S_A^* \leftrightarrow S_C^*$ transition at 130 °C (Figure

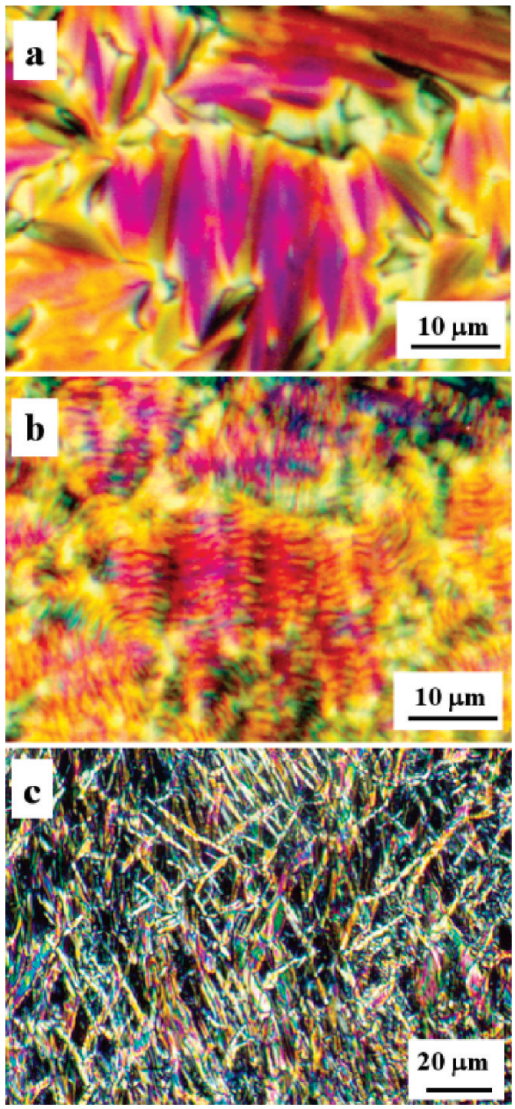

Figure 7. PLM pictures of S_A^*, S_C^*, and TGBA phases.[45]

7b). The broken focal conics are indicative of the S_C^* phase which is consistent with 2D WAXD fiber pattern results. The formation of this broken texture is due to the shrinkage of layer thickness from chain tilting during the transition.[45]

The remaining issue is the LC phase that appears at high temperatures between two higher temperature first-order transitions as shown in Figures 3 and 4. For PET(R*-9), as an example, the highest temperature phase after the exothermic process is the isotropic melt, while below 175 °C it is the S_A^* phase. On the basis of the WAXD results, one can conclude that the undetermined phase must also be related to the S_A^* phase since the low angle reflection at $2\theta = 3.0°$, which represents the layer structure, starts to appear at 185 °C in the 1D WAXD patterns as shown in Figure 5. Since neither the 1D WAXD, nor the 2D WAXD fiber patterns are sensitive to the structural changes at this transition, one speculates that this transition must be related to a larger length scale supra-molecular assembly rather than a structure change on the molecular scale. The observations obtained by PLM show helical textures with alternating strong and weak birefringence as shown in Figure 7c. This LC morphology is virtually identical to the twisted grain boundary (TGB) phase morphology observed in small molecule LC and side-chain LC polymers.[25,45−52] Combining both observations of the PLM helical texture and the WAXD

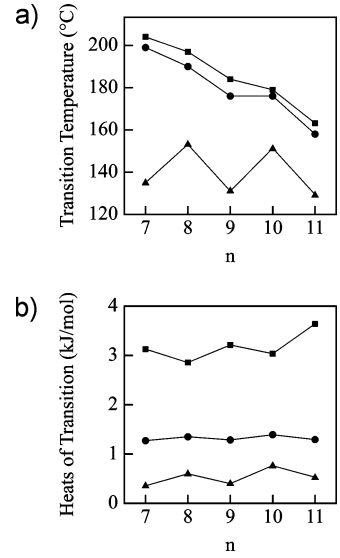

Figure 8. Odd−even effects on the LC phase transition temperatures (a) and heats of transitions for PETs(R*-*n*) (b): (▲) $S_C^* \leftrightarrow S_A^*$; (•) $S_A^* \leftrightarrow$ TGBA*; (■) I.[46]

results, it is strongly suggested that the high temperature phase between the isotropic melt and the S_A^* phase is a TGBA* phase.

After examining the complete series of PET(R*-*n*) (n = 7−11) samples, we have observed an odd−even effect on thermodynamic transition properties.[37] The odd−even effects are shown in Figure 8a and b, which include the $S_C^* \leftrightarrow S_A^*$, $S_A^* \leftrightarrow$ TGBA*, and TGBA* ↔ I phase transitions.[46] Figure 8a indicates that the LC phase transition temperatures of the PET(R*-odd) polymers are lower than those of the PETs(R*-even) polymers. Furthermore, this odd−even effect is stronger in the formation of the S_C^* phase than in the formation of the S_A^* and TGBA* phases. In Figure 8b, the heats of transition for the $S_C^* \leftrightarrow S_A^*$ and the $S_A^* \leftrightarrow$ TGBA* transitions also exhibit identical trends. The odd−even effect is much stronger in the $S_C^* \leftrightarrow S_A^*$ transition than in the $S_A^* \leftrightarrow$ TGBA* transition. Specifically, in the TGBA* ↔ I transitions, the heat of transition of PETs(R*-odd) are higher than those of PETs(R*-even), contrary to the odd−even effect on the heats of transitions observed for the other two phase transitions. At this moment, it is not clear why this abnormal odd−even effect behavior takes place. One expects that this may be associated with the total number of atoms in the polymer backbone spacers and their different packing modes.[46]

Identification of Crystalline Phases. Crystallization occurs between the T_g and T_m. For PET(R*-9), the crystallization window is between 37 and 170 °C. Within this crystallization window, the S_A^* phase covers the 130 to 175 °C temperature region, while the S_C^* phase covers the 37 to 130 °C region. As shown in Figure 9 for PET(R*-9), when the heating rate is slow (≤5 °C/min), crystallization occurs. Figure 10 shows a set of 1D WAXD powder patterns recorded during heating at 1 °C/min for a quenched PET(R*-9) sample. When the temperature reaches 80 °C, multiple reflections start to appear in the wide-angle region, indicating that crystallization is initiated. These reflections remain until the temperature approaches 170 °C, where the crystal melts. The crystal structure developed from both the S_A^* and S_C^* phases are identical yet with different orientations in uniaxially deformed samples.[45]

The crystal structure is traditionally determined utilizing selected area electron diffraction (SAED) and WAXD techniques. Figure 11 shows a 2D WAXD fiber pattern for a

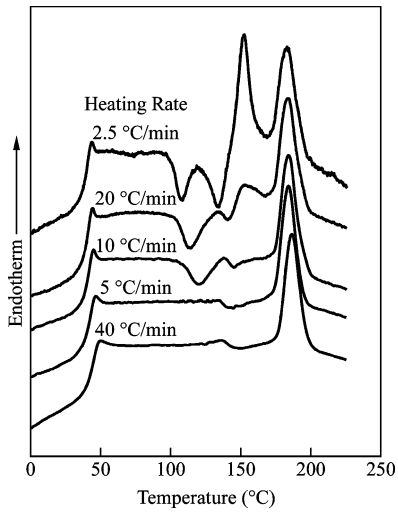

Figure 9. Set of DSC heating thermodiagrams at different rates between 2.5 and 40 °C/min for PET(R*-9).[45]

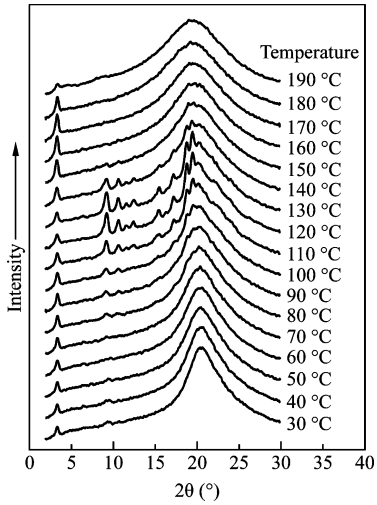

Figure 10. Set of 1D WAXD patterns at different temperatures at a heating rate of 1 °C/min for a quenched PET(R*-9) sample.[45]

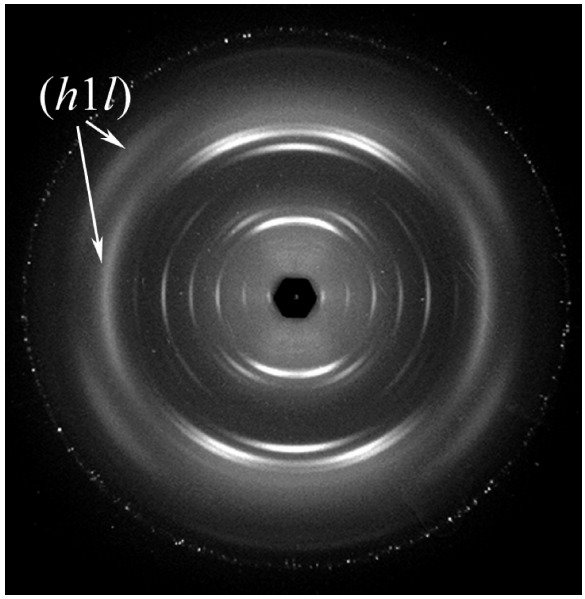

Figure 11. 2D WAXD pattern (a) and a SAED pattern (b) of a PET(R*-9) sample.[45]

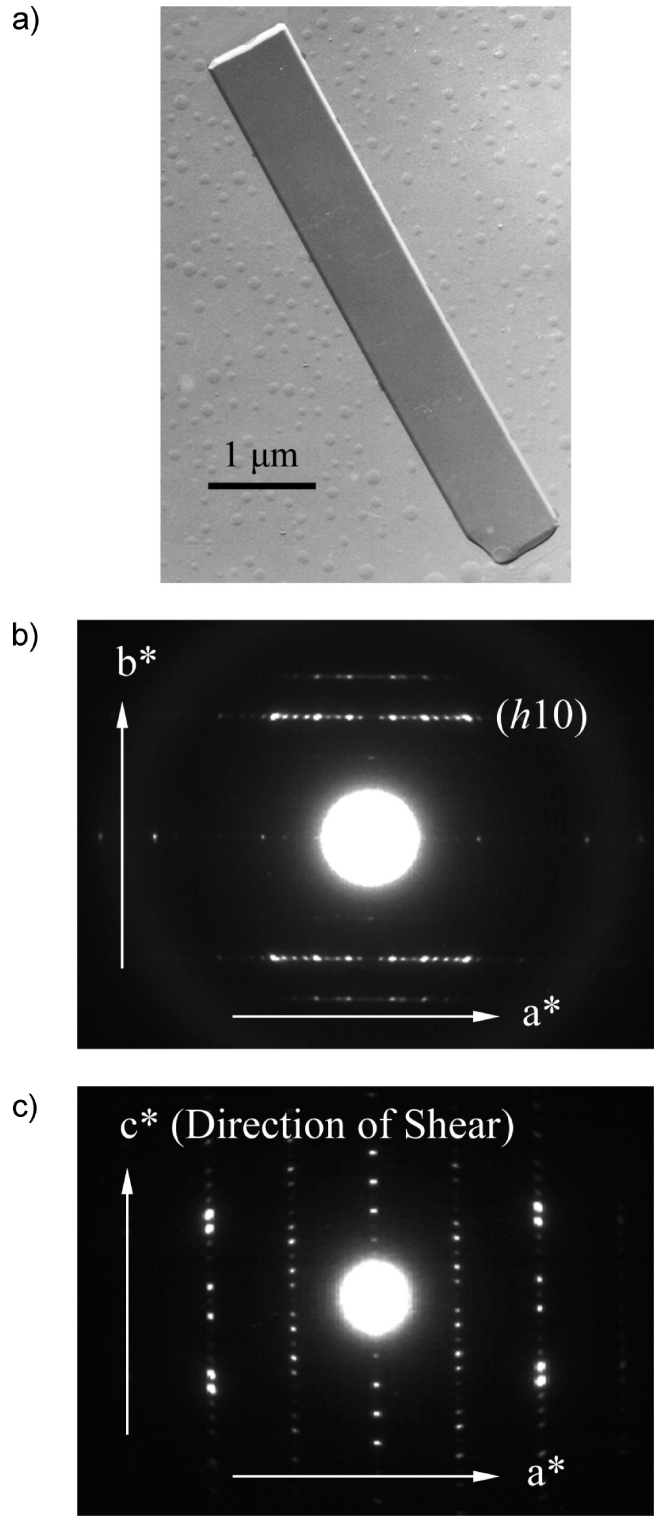

Figure 12. TEM bright field image of a "curved flat" single crystal of the PET(R*-9) sample (a), the corresponding [100] zone SAED pattern (b), and the [010] zone SAED pattern on a single crystal grown from sheared sample (c).[41]

PET(R*-9) sample that has been annealed at 145 °C for one day and then quenched to room temperature. This figure exhibits multiple reflections. Along the equator, up to six diffraction orders exist for the (00*l*) planes. Therefore, the *c*-axis dimension was determined to be 5.96 nm.[45] Interestingly enough, the *c*-axis is along the equator rather than along the meridian, an often observed phenomenon in biomaterial fibers.[10] However, this kind of molecular orientation in biomaterial fibers is perhaps

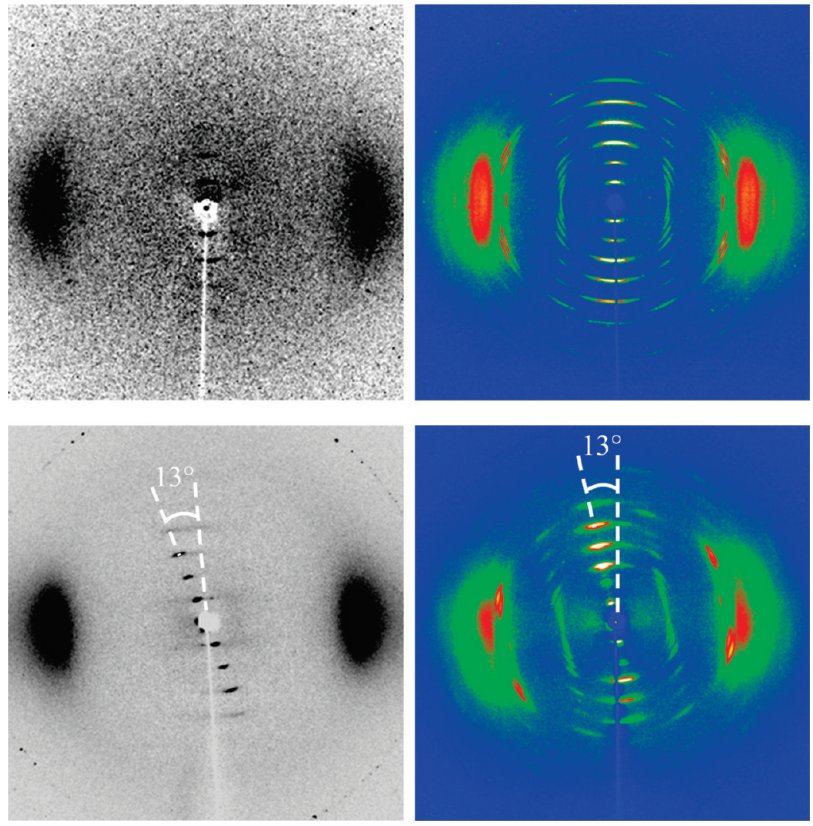

Figure 13. 2D WAXD patterns for uniaxially elongated PET(R*-7) samples: (a) elongated at 145 °C; (b) elongated and annealed at 145 °C for 5 days; (c) elongated at 135 °C; (d) elongated and annealed at 135 °C for 5 days. The arrow indicates the direction of elongation.[54]

due to the existence of the parallel and antiparallel hydrogen bond interactions between the chain molecules and their supramolecular β-sheets. The origin of this anomalous 2D WAXD pattern in PET(R*-9) fibers may be associated with the fact that they were drawn from the S_A^* phase, similar to the example of a series of poly(ester imide)s reported recently[53] and could be linked to the low molecular weight of the material.

The meridian of the PET(R*-9) fiber pattern in Figure 11 has been assigned as the a^* direction. In the quadrants, three layers of reflections can be observed. The first ($1kl$), the second ($2kl$), and the third ($3kl$) layers (since the meridian direction is defined as the a^*-direction) display six, four, and one diffraction, respectively. The ($h1l$) diffractions are relatively weak and diffuse as shown in Figure 11 (see arrows in the figure). This may possibly be due to the superstructure formed as discussed in previous publications.[41,42]

Detailed assignment of those diffractions and unit cell symmetry require different zones obtained from SAED. The key issue to obtain these ED patterns is to grow sizable single crystals of this series of polymers. Figure 12a shows a "curved flat" single crystal of PET(R*-9) grown thermotropically at 145 °C in a thin film sample.[42] A [$00l$] zone SAED pattern of this flat lamellar crystal is shown in Figure 12b. The pattern in this figure thus represents the a^*b^* two-dimensional lattice, and the b^*-axis is along the long axis of the lamellar crystal shown in Figure 12a. The unit cell dimensions were determined to be a = 1.07 nm and b = 0.48 nm. The c-axis dimension can be determined through either a series of ED patterns from different zones obtained by tilting along both the a^* and b^* axes or, an SAED pattern from the [010] zone.[42] Figure 12c shows such a [010] zone ED pattern, which represents the a^*c^* reciprocal plane consisting of the ($h0l$) diffractions. The dimensions of both axes are in excellent agreement with the results derived from the ED pattern shown in Figure 12b and the WAXD pattern shown in Figure 11.[32,41,42,46] The crystal lattice was determined to be orthorhombic with dimensions of a = 1.07, b = 0.48, and c = 5.96 nm.[28,32,41,42] In Figure 12c, the (201), (205), and (206) reflections marked in this figure will be critical in understanding the molecular packing in helical object which will be discusses later in this article.

The unit cell of both PET(R*-7) and PET(R*-11), based on both WAXD fiber patterns and SAED patterns, was determined to be monoclinic. For PET(R*-7), the unit cell dimensions were found to be a = 1.04, b = 0.46, and c = 5.59 nm and γ = 84.2°.[54] For PET(R*-11), the unit cell parameters were a = 1.03, b = 0.47, and c = 64.3 nm and γ = 83°.[46]

As indicated in a recent report, the molecular arrangement in the different LC phases has a significant impact on the crystallization process.[54] The $S_C^* \leftrightarrow S_A^*$ transition temperature is 139 °C for PET(R*-7). When uniaxially elongated at 145 °C, the film sample gives a typical 2D WAXD pattern of the S_A^* phase as shown in Figure 13a. The elongation direction is along the meridian, on which the layer diffraction of the S_A^* phase appears up to the third order. Amorphous halos on the equator indicate that the mesogen orientation is parallel to the layer normal. When the film is elongated and annealed at the same temperature for 5 days, crystalline reflections appear in the quadrants as shown in Figure 13b. In this figure, the amorphous halos remain on the equator while layer diffractions remain along the meridian, revealing that the noncrystalline part of the sample is still in the S_A^* phase, and the c^*-axis of the crystals is parallel to the meridian, namely, the layer normal of the S_A^* phase. When the film sample is elongated at 135 °C, the layer reflections tilt 13° away from the meridian, while the amorphous halos remain on the equator (Figure 13c). This is a typical 2D WAXD pattern for a S_C^* phase (the S_C^* phase of this

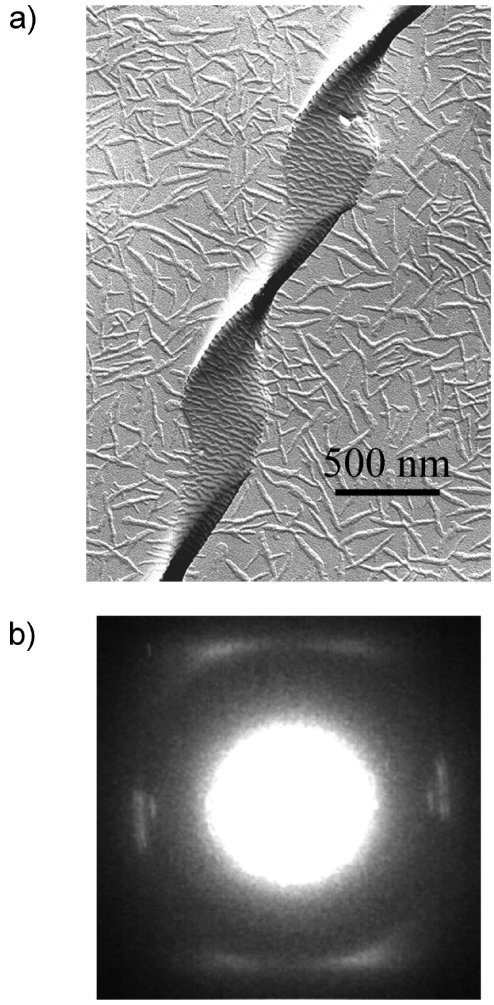

Figure 14. Right-handed lamellar helical crystal of the PET(R*-9) sample (a) and the corresponding SAED pattern (b).[28]

sample is synclinic with the mesogens tilted 21° away from the layer normal, see ref 54 for detailed discussion). When the PET(R*-7) film sample is elongated and annealed at 135 °C for 5 days, the *c**-axis of the crystalline diffraction pattern also tilts 13° away from the meridian. As shown in Figure 13d, all the diffraction pairs are tilted except for the amorphous halos, indicating that the *c*-axis of the crystals retains the mesogen orientation from the S_C^* phase. It can thus be concluded that the chain orientation of isothermally grown crystals is the same as the chiral smectic phase from which the crystals grow. This study illustrates the confinement effect of the nonracemic chiral LC phases on the growth of crystals and thus provides information on the crystallization mechanism.

Helical Lamellar Crystals and Double-Twisted Mechanism. Helical single lamellar crystals have been thermotropically grown under crystallization conditions that also yield flat lamellar crystals. Figure 14a shows a helical crystal grown at 145 °C for PET(R*-9).[28,32,41,42] Right-handed helical crystals, as shown in Figure 14a, are exclusively observed for this particular polymer. Figure 14b is a SAXD pattern of this helical crystal. On the basis of our ED experiments, surprisingly, flat and twisted crystals possess the same structure. The polymer chain folding direction in both flat and helical lamellar crystals is always along the long axis of the lamellar crystals, as determined by polyethylene decoration.[41]

The ED pattern of Figure 14b displays only arced diffractions as a result of crystal twisting. There are three diffraction arcs

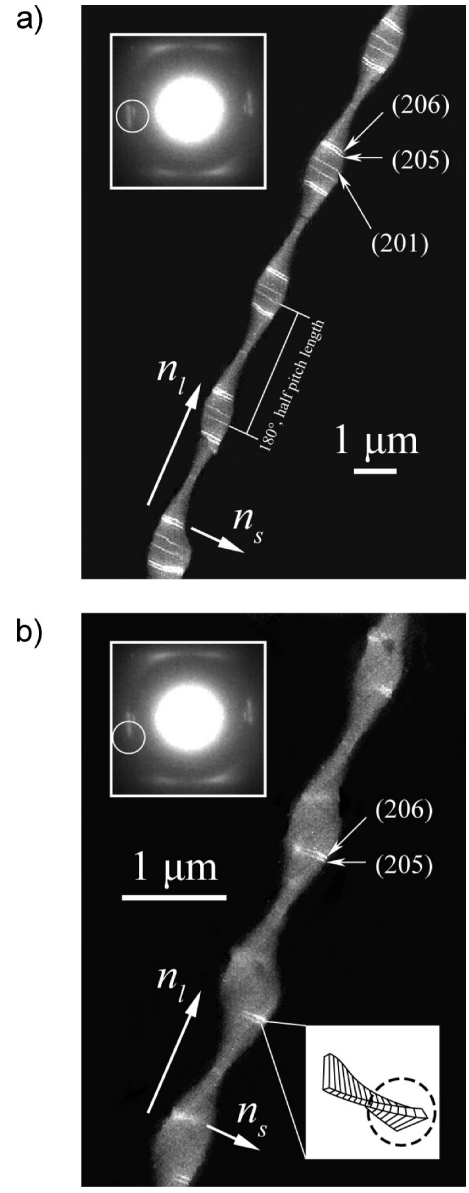

Figure 15. TEM DF image of the helical crystal from the entire (201), (205), and (206) arcs (a) and partial arcs which are circled in the figure (b).[28]

along the horizontal direction, namely the (201), (205) and (206) arcs (see also in Figure 12c).[28,32,41,42] If all three arcs are selected to perform a dark field (DF) imaging in TEM, sets of bright bands appear across the short axis (n_s) of the helical crystal as shown in Figure 15a. The bright bands are twisted along the long axis (n_l) of the helical crystal, resulting in either a 5°, 25°, or 30° tilt from the substrate. Note that the half pitch length along the n_l axis requires a 180° twist. In explaining the DF results shown in Figure 15a, we need to assume a twisting model to describe the chain orientation in the crystals. There are two possible models: the single-twist model (only along the n_l axis) and the double-twist model (along both the n_l and n_s axes) as shown in Figure 16a and b.[28,32]

In order to determine whether the single-twist or double-twist model is accurate, we conducted another TEM DF experiment, in which only part of the diffraction arcs was used to construct the DF image. If the single-twist model works, these three bright bands across the n_s axis of the helical crystal should still be observed, but their intensities should decrease by half. If the double-twist model is correct, only half of each of the bright

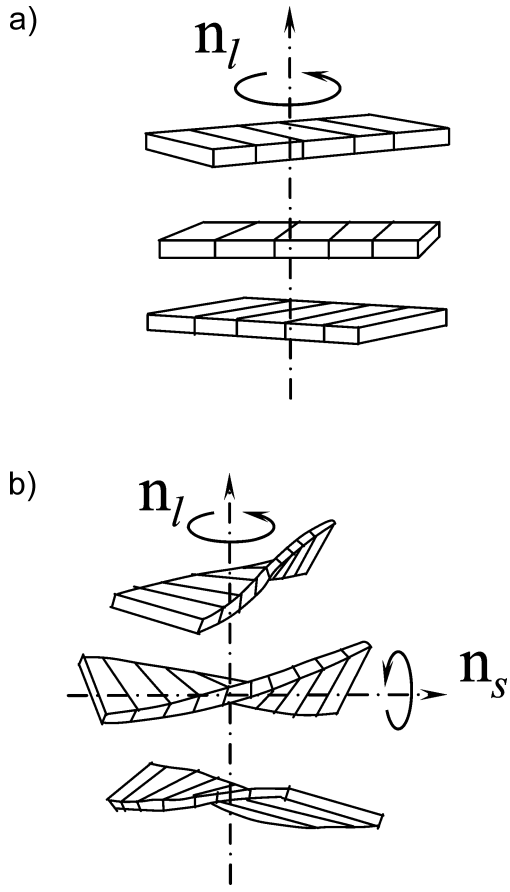

Figure 16. Schematic drawing of the single-twist model (a) and the double-twist model (b) for the helical crystals.[28]

bands from these three diffractions should be observed in the DF image. The result shown in Figure 15b supports the double-twisted chain orientation in the helical crystal. Namely, the chain molecules are not only twisted along the n_l axis but also along the n_s axis. Quantitatively, the twist direction along the n_l axis results from a rotation of successive molecular layers of approximately 0.05°.[28,32] The twisted direction along the n_s axis indicates a rotation of approximately 0.01° per molecular layer. On the basis of these experimental observations, the concept of a *double-twist* molecular orientation in the helical lamellar crystal was introduced, although, in principle, the macroscopic translation symmetry in the helical crystal is broken along both the long and short axes. This crystal can therefore be recognized to be "soft", rather than a true crystal based on the traditional crystal definition in Euclidean space.[55] Mathematically, double-twist crystals can only be true crystals in Riemannian space.[28,32,56]

Furthermore, the helical lamellar crystals are right-handed for PET(R*-9). For PET(L*-9), the helical crystal handedness changes to left-handed,[49] indicating that the primary configurational chirality affects the tertiary phase chirality. However, for PET(R*-*n*) polymers when *n* is odd ($n = 7$, 9, and 11), the helical lamellar crystals are right-handed, while the helical handedness becomes left-handed when *n* is even ($n = 8$ and 10). In other words, in addition to the odd−even effect on thermodynamic properties of the phase transitions, we have also found a profound impact of the odd−even effect on helical handedness on the length scale of the tertiary chiral structure. This observation clearly indicates that the primary configurational chirality is important, but it is not the only factor that

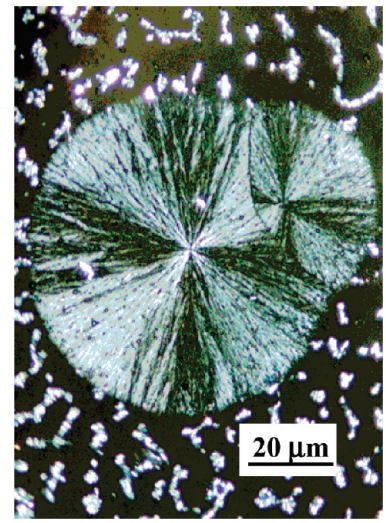

Figure 17. PLM micrograph of a spherulite of PET(R*-10) grown from the melt at 130 °C.[57]

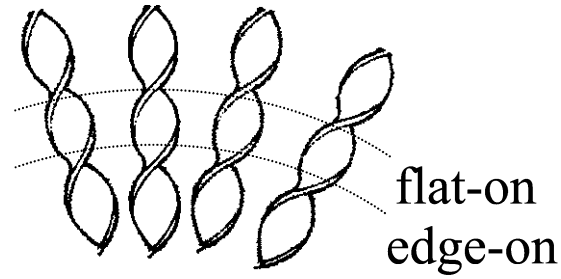

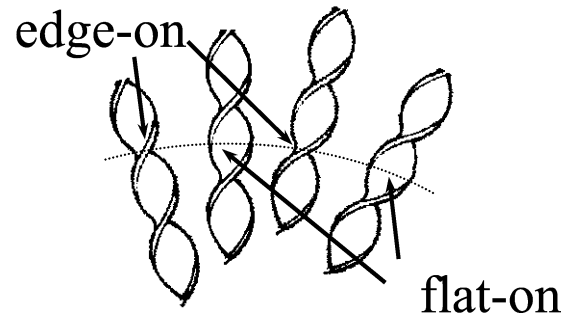

Figure 18. Schematic drawing of packing schemes of individual lamellae to form spherulites: (a) cooperative packing; (b) noncooperative packing.[57]

determines the chirality handedness of longer length scales. This phenomenon has been discussed in one of our recent publications.[57]

Nonbanded Spherulitic Structure: A Loss of the Quaternary Object Chirality. Figure 17 is the PLM micrograph of a relatively thick sample of PET(R*-10) crystallized at 130 °C. The spherulitic morphology can clearly be seen. However, this spherulite does not possess the banded texture usually observed in crystalline polymers. This indicates that a cooperative lamellar twisting of PET(R*-10) does not occur in the formation of this spherulite.[58] Is this indicative of a failure to transfer chirality from the tertiary to the quaternary chiral structure levels? We need to be aware that helical single lamellar crystals may not automatically pack into cooperative twisting lamellar stacks and, therefore, do not form spherulites with a banded texture. Figure 18a schematically illustrates the traditional mechanism of forming a spherulite with a banded texture. In a helical lamellar crystal, the edge-on and the flat-on parts

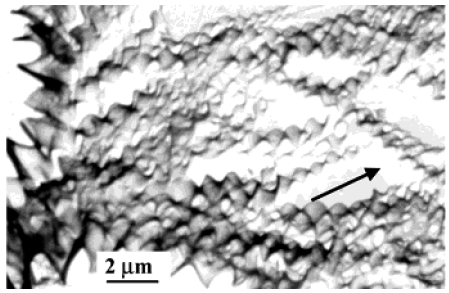

Figure 19. TEM morphology of a PET(R*-10) spherulite observed via the replica method. The growth direction of this spherulite is indicated by the arrow.[57]

of the crystal have different birefringence due to different refractive indices along the three axes of the crystal unit cell. When lamellar crystals are stacked cooperatively and twist together, all edge-on and flat-on arrangements are in plane along the growth direction, and a banded texture with alternating dark and bright birefringence is formed. However, if the lamellar crystals twist individually rather than cooperatively, the dark and bright bands exist in each individual lamella, but the overall cooperative twisting is lost as shown in Figure 18b which schematically represents a noncooperative packing scheme in the helical lamellar crystals. Since the resolution of PLM does not permit the observation of this birefringence change for the individual lamella, the macroscopic banded texture cannot be observed.

This argument can be supported by carrying out an experiment in which PET(R*-10) crystallizes from a concentrated solution, and the solvent continuously evaporates during crystallization. Figure 19 shows a precursor of a spherulite made of many helical crystals. However, these individual helical crystals do not pack in a cooperative way to form twisted lamellar stacks.[58] Therefore, no macroscopic banded texture can be observed. It is evident that between these two chiral structural length scales, again, the packing scheme of the helical lamellar single crystals is a determining factor to enable the chirality transfer into the object chiral structures, here into spherulites.

Conclusion

In summary, we have found that chirality at higher levels is ultimately the outcome of a cascade of chiralities that exist on smaller length scales: a chiral center, conformational chirality, helical lamellar single crystal, and object chirality. Chirality transfer from one length scale to another is neither automatic, nor necessary. Chirality transfer depends critically upon the packing scheme of the chiral building blocks on each length scale. A parallel and noncooperative packing scheme stops this chirality transfer process, while a nonparallel and cooperative packing scheme advances the process.

Acknowledgment

This work was supported by the NSF (DMR-0516602 and DMR-0906898).

Literature Cited

(1) Bassett, D. C.; Frank, F. C.; Keller, A. Lamellae and their organization in melt-crystallized polymers. *Philos. Trans. Roy. Soc. London* **1994**, *A348*, 29–43.

(2) Keith, H. D.; Padden, F. J., Jr. Banding in polyethylene and other spherulites. *Macromolecules* **1996**, *29*, 7776–7786.

(3) Singfield, K. L.; Klass, J. M.; Brown, G. R. Optically active polyethers. 2. Atomic force microscopy of melt-crystallized poly(epichlorohydrin) enantiomers and their equimolar blend. *Macromolecules* **1995**, *28*, 8006–8015.

(4) Singfield, K. L.; Hobbs, J. K.; Keller, A. Correlation between main chain chirality and crystal "twist" direction in polymer spherulites. *J. Cryst. Growth* **1998**, *183*, 683–689.

(5) Saracovan, I.; Cox, J. K.; Revol, J.-F.; Manley, R. St. J.; Brown, G. R. Optically active polyethers. 3. On the relationship between main-chain chirality and the lamellar morphology of solution-grown single crystals. *Macromolecules* **1999**, *32*, 717–725.

(6) Saracovan, I.; Keith, H. K.; Manley, R. St. J.; Brown, G. R. Banding in spherulites of polymers having uncompensated main-chain chirality. *Macromolecules* **1999**, *32*, 8918–8922.

(7) Marsh, R. E.; Corey, R. B.; Pauling, L. An investigation of the structure of silk fibroin. *Biochim. Biophys. Acta* **1955**, *16*, 1–34.

(8) Lucas, F.; Shaw, J. T.B.; Smith, S. G. The amino acid sequence in a fraction of the fibroin of *Bombyx mori*. *Biochem. J.* **1957**, *66*, 468–479.

(9) Chothia, C. Conformation of twisted β-pleated sheets in proteins. *J. Mol. Biol.* **1973**, *75*, 295–302.

(10) Chothia, C.; Levitt, M.; Richardson, D. Structure of proteins: packing of alpha-helices and pleated sheets. *Proc. Natl. Acad. Sci. U.S.A.* **1977**, *74*, 4130–4134.

(11) Lotz, B.; Gonthier-Vassal, A.; Brack, A.; Magoshi, J. Twisted single crystals of *Bombyx mori* silk fibroin and related model polypeptides with β structure: A correlation with the twist of the β sheets in globular proteins. *J. Mol. Biol.* **1982**, *156*, 345–357.

(12) Livolant, F.; Bouligand, Y. Double helical arrangement of dinoflagellate chromosomes. *Chromosoma* **1980**, *80*, 97–118.

(13) Keith, H. D.; Padden, F. J., Jr.; Lotz, B.; Wittmann, J. C. Asymmetries of habit in polyethylene crystals grown from the melt. *Macromolecules* **1989**, *22*, 2230–2238.

(14) Oda, R.; Huc, I.; Schmutz, M.; Candau, S. J.; MacKintosh, F. C. Tuning bilayer tweist using chiral counterions. *Nature* **1999**, *399*, 566–568.

(15) (a) For a recent review on experimental observations, see Brizard, A.; Oda, R.; Huc, I. Chirality effects in self-assembled fibrillar networks. *Top. Curr. Chem.* **2005**, *256*, 167–218. (b) A review on theoretical studies is given by Selinger, J. V.; Spector, M. S.; Schnur, J. M. Theory of self-assembled tubules and helical ribbons. *J. Phys. Chem. B* **2001**, *105*, 7157–7169.

(16) Lindsell, W. E.; Preston, P. N.; Seddon, J. M.; Rosair, G. M.; Woodman, T. A. J. Macroscopic helical and cylindrical morphologies from achiral 1,3-diynes. *Chem. Mater.* **2000**, *12*, 1572–1576.

(17) Cornelissen, J. J. L. M.; Fischer, M.; Sommerdijk, N. A. J. M.; Nolte, R. J. M. Helical superstructures from charged poly(styrene)-poly(isocyanodipeptide) block copolymers. *Science* **1998**, *280*, 1427–1430.

(18) Yan, L.; Tao, W. Synthesis of achiral PEG-PANI rod-coil block copolymers and their helical superstructures. *J. Polym. Sci., Polym. Chem.* **2008**, *46*, 12–20.

(19) Goodby, J. W.; Slaney, A. J.; Booth, C. J.; Nishiyama, I.; Vuijk, J. D.; Styring, P.; Toyne, K. J. Chirality and frustration in ordered fluids. *Mol. Cryst. Liq. Cryst.* **1994**, *243*, 231–298.

(20) Kaspar, M.; Gorecka, E.; Sverenyak, H.; Hamplova, V.; Glogarova, M.; Pakhomov, S. A. Helix twist inversion in ferroelectric liquid crystals with one chiral centre. *Liq. Cryst.* **1995**, *19*, 589–594.

(21) Saupe, A. Recent results in the field of liquid crystals. *Angew. Chem. Intl. Ed.* **1968**, *7*, 97–112.

(22) Buckingham, A. D.; Ceasar, G. P.; Dunn, M. B. The addition of optically active compounds to nemetic liquid crystals. *Chem. Phys. Lett.* **1969**, *3*, 540–541.

(23) de Gennes, P. G. An analogy between superconductors and smectics A. *Solid State Commun.* **1972**, *10*, 753–756.

(24) Renn, S. R.; Lubensky, T. C. Abrikosov dislocation lattice in a model of the cholesteric-to-smectic-A transition. *Phys. Rev. A* **1988**, *38*, 2132–2147.

(25) (a) Goodby, J. W.; Waugh, M. A.; Stein, S. M.; Chin, E.; Pindak, R.; Patel, J. S. A new molecular ordering in helical liquid crystals. *J. Am. Chem. Soc.* **1989**, *111*, 8119–8125. (b) Goodby, J. W.; Waugh, M. A.; Stein, S. M.; Chin, E.; Pindak, R.; Patel, J. S. Characterization of a new helical smectic liquid crystal. *Nature* **1989**, *337*, 449–451.

(26) Helfrich, W.; Oh, C. S. Optically active smectic liquid crystal. *Mol. Cryst. Liq. Cryst.* **1971**, *14*, 289–292.

(27) Saupe, AOn molecular structure and physical properties of thermotropic liquid crystals. *Mol. Cryst. Liq. Cryst.* **1969**, *7*, 59–74.

(28) Li, C. Y.; Cheng, S. Z. D.; Ge, J. J.; Bai, F.; Zhang, J. Z.; Mann, I. K.; Harris, F. W.; Chien, L.-C.; Yan, D.; He, T.; Lotz, B. Double twist in helical polymer "soft" crystals. *Phys. Rev. Lett.* **1999**, *83*, 4558–4561.

(29) Kléman, M. Defects in liquid crystals. *Rep. Prog. Phys.* **1989**, *52*, 555–654.

(30) For a recent summary, see Livolant, F. Precholesteric liquid crystalline states of DNA. *J. Phys. (Paris)* **1987**, *48*, 1051–1066.

(31) Livolant, F.; Leforestier, A. Condensed phases of DNA: Structures and phase transitions. *Prog. Polym. Sci.* **1996**, *21*, 1115–1164.

(32) Li, C. Y.; Cheng, S. Z. D.; Ge, J. J.; Bai, F.; Zhang, J. Z.; Mann, I. K.; Chien, L.-C.; Harris, F. W.; Lotz, B. Molecular orientation in flat-elongated and helical lamellar crystals in a main-chain nonracemic chiral polyester. *J. Am. Chem. Soc.* **2000**, *122*, 72–79.

(33) Lotz, B.; Cheng, S. Z. D. A critical assessment of unbalanced surface stresses as the mechanical origin of twisting and scrolling of polymer crystals. *Polymer* **2005**, *46*, 577–610.

(34) Ho, R.-M.; Chiang, Y.-W.; Tsai, C.-C.; Lin, C.-C.; Ko, B.-T.; Huang, B.-H. Three-dimensionally packed nanohelical phase in chiral block copolymers. *J. Am. Chem. Soc.* **2004**, *126*, 2704–2705.

(35) Chiang, Y.-M.; Ho, R.-M.; B. T. Ko, B.-T.; Lin, C. C. Springlike nanohelical structures in chiral block copolymers. *Angew. Chem., Int. Ed.* **2005**, *44*, 7969–7972.

(36) Ho, R.-M.; Chiang, Y.-M.; Chen, C.-K.; Wang, H.-W.; Hasegawa, H.; Akasaka, S.; Thomas, E. L.; C. Burger, C.; B. S. Hsiao, B. S. Block copolymers with a twist. *J. Am. Chem. Soc.* **2009**, *131*, 18533–18542.

(37) Ho, R.-M.; Chiang, Y.-W.; Lin, S.-C.; Chen, C.-K. Helical architectures from self-assembly of chiral polymers and block copolymers. *Prog. Polym. Sci.*, **2010**, in press.

(38) Jeong, K.-U.; Jin, S.; Ge, J. J.; Knapp, B. S.; Graham, M. J.; Ruan, J.; Guo, M.; Xiong, H.; Harris, F. W.; Cheng, S. Z. D. Phase structures and self-assembled helical suprastructures via hydrogen bonding in a series of achiral 4-biphenyl carboxylic acid compounds. *Chem. Mater.* **2005**, *17*, 2852–2865.

(39) Jeong, K.-U.; Ge, J. J.; Jin, S.; Knapp, B. S.; Graham, M. J.; Harris, F. W.; Cheng, S. Z. D. Origin of self-assembled helical supramolecular structures in achiral C6 biphenyl carboxylic acid compounds. *Chem. Mater.* **2006**, *18*, 680–690.

(40) Jeong, K.-U.; Yang, D.; Graham, M. J.; Tu, Y.; Kuo, S.-W.; Knapp, B. S.; Harris, F. W.; Cheng, S. Z. D. Construction of chiral propeller architectures from achiral molecules. *Adv. Mater.* **2006**, *18*, 3229–3232.

(41) Li, C. Y.; Yan, D.; Cheng, S. Z. D.; Bai, F.; He, T.; Chien, L.-C.; Harris, F. W.; Lotz, B. Double-twisted helical lamellar crystals in a synthetic main-chain polyester similar to biological polymers. *Macromolecules* **1999**, *32*, 524–527.

(42) Li, C. Y.; Yan, D.; Cheng, S. Z. D.; Bai, F.; Ge, J. J.; Calhoun, B. H.; He, T.; Chien, L.-C.; Harris, F. W.; Lotz, B. Helical single-lamellar crystals thermotropically formed in a synthetic nonracemic chiral main-chain polyester. *Phys. Rev. B* **1999**, *60*, 12675–12680.

(43) Bai, F.; Chien, L.-C.; Li, C. Y.; Cheng, S. Z. D.; Petschek, R. Synthesis and characterization of isoregic chiral smectic polyesters. *Chem. Mater.* **1999**, *11*, 1666–1671.

(44) Economy, J.; Storm, R. S.; Matkovich, V. I.; Cottis, S. G.; Nowak, B. E. Synthesis and structure of the *p*-hydroxybenzoic acid polymer. *J. Polym. Sci. Polym. Chem. Ed.* **1976**, *14*, 2207–2224.

(45) Li, C. Y.; Ge, J. J.; Bai, F.; Zhang, J. Z.; Calhoun, B. H.; Chien, L.-C.; Harris, F. W.; Lotz, B.; Cheng, S. Z. D. Phase transformations in a chiral main-chain liquid crystalline polyester involving double-twist helical crystals. *Polymer* **2000**, *41*, 8953–8960.

(46) Weng, X.; Li, C. Y.; Jin, S.; Zhang, D.; Zhang, J. Z.; Bai, F.; Harris, F. W.; Cheng, S. Z. D.; Lotz, B. Helical twist senses, liquid crystalline behavior, crystal microtwins, and rotation twins in a polyester containing main-chain molecular asymmetry and effects of the number of methylene units in the backbones on the phase structures and morphologies of its homologues. *Macromolecules* **2002**, *35*, 9678–9686.

(47) Ge, J. J.; Honigfort, P. S.; Ho, R.-M.; Wang, S.-Y.; Harris, F. W.; Cheng, S. Z. D. Phase structures, transition behavior and surface alignment in polymers containing rigid rod-like backbones with flexible side chains. 3. The even-odd effect on phase trasitions in combined liquid crystal polyesters. *Macromol. Chem. Phys.* **1999**, *200*, 31–43.

(48) Pardey, R.; Zhang, A.; Gabori, P. A.; Harris, F. W.; Cheng, S. Z. D.; Adduci, J.; Facinelli, J. V.; Lenz, R. W. Monotropic liquid crystal behavior in two poly(ester imides) with even and odd flexible spacers. *Macromolecules* **1992**, *25*, 5060–5068.

(49) Pardey, R.; Shen, D.; Gabori, P. A.; Harris, F. W.; Cheng, S. Z. D.; Adduci, J.; Facinelli, J. V.; Lenz, R. W. Ordered structures in a series of liquid-crystalline poly(ester imides). *Macromolecules* **1993**, *26*, 3687–3697.

(50) Yoon, Y.; Zhang, A.; Ho, R.-M.; Cheng, S. Z. D.; Percec, V.; Chu, P. Phase identification in a series of liquid crystalline TPP polyethers and copolyethers having highly ordered mesophase structures. 1. Phase diagrams of odd-numbered TPP polyethers. *Macromolecules* **1996**, *29*, 294–305.

(51) Yoon, Y.; Ho, R.-M.; Moon, B.; Kim, D.; McCreight, K. W.; Li, F.; Harris, F. W.; Cheng, S. Z. D.; Percec, V.; Chu, P. Mesophase identifications in a series of liquid crystalline TPP polyethers and copolyethers having highly ordered mesophase structures. 2. Phase diagram of even-numbered polyethers. *Macromolecules* **1996**, *29*, 3421–3431.

(52) Bolton, E. C.; Lacey, D.; Smith, P. J.; Goodby, J. W. Twisted smectic A phase in side chain liquid crystal polymers. *Liq. Cryst.* **1992**, *12*, 305–318.

(53) Leland, M.; Wu, Z.; Chhajer, M.; Ho, R.-M.; Cheng, S. Z. D.; Keller, A.; Kricheldorf, H. R. Anomalous orientation behavior in a series of copoly(ester imide)s observed by wide-angle X-ray diffraction. *Macromolecules* **1997**, *30*, 5249–5254.

(54) Jin, S.; Jeong, K.-U.; Tu, Y.; Graham, M. J.; Wang, J.; Harris, F. W.; Cheng, S. Z. D. Structure of macroscopic monodomains and its soft confinements of chiral smectic phases on crystallization in a main-chain nonracemic liquid crystalline polyester. *Macromolecules* **2007**, *40*, 5450–59.

(55) The latest definition of crystal, provided by the International Union of Crystallography to account for the discovery of quasicrystals, reads: "by 'crystal' we mean any solid having an essentially discrete diffraction diagram, and by 'aperiodic crystal' we mean any crystal in which three-dimensional lattice periodicity can be considered to be absent." (International Union of Crystallography *Acta Crystallogr.* **1992**, *A48*, 922.) However, even eliminating the criteria of three-dimensional periodicity, such a working definition is not general enough to include our helical crystal, since the diffraction patterns are continuous arcs in Euclidean space, not a discrete diffraction diagram. But, in curved space, a pure point Fourier spectrum (discrete diffraction) can be obtained which would fulfill the necessary and sufficient condition to define the helical crystal as a true crystal.

(56) Li, C. Y.; Ge, J. J.; Bai, F.; Calhoun, B. H.; Harris, F. W.; Chien, L.-C.; Lotz, B.; Keith, H. D. Early-stage formation of helical single crystals and their confined growth in thin film. *Macromolecules* **2001**, *34*, 3634–3641.

(57) Li, C. Y.; Cheng, S. Z. D.; Weng, X.; Ge, J. J.; Bai, F.; Zhang, J. Z.; Calhoun, B. H.; Harris, F. W.; Chien, L.-C.; Lotz, B. Left or right, it is a matter of one methylene unit. *J. Am. Chem. Soc.* **2001**, *123*, 2462–2463.

(58) Li, C. Y.; Jin, S.; Weng, X.; Ge, J. J.; Zhang, D.; Bai, F.; Harris, F. W.; Cheng, S. Z. D.; Yan, D.; T. He, T.; Lotz, B.; Chien, L.-C. Liquid crystalline phases, microtwinning in crystals and helical chirality transformations in a main-chain chiral liquid crystalline polyester. *Macromolecules* **2002**, *35*, 5475.

Received for review February 1, 2010
Revised manuscript received March 11, 2010
Accepted March 18, 2010

IE100248R